Journal of Engineering Mathematics **50:** 51–74, 2004.

Intrinsic dynamics of the boundary of a two-dimensional uniform vortex

GIORGIO RICCARDI
Department of Aerospace and Mechanical Engineering, Second University of Naples, via Roma, 29 - 81031 *Aversa (CE), Italy; E-mail address: giorgio.riccardi@email.it*

Received 1 April 2003; accepted in revised form 1 March 2004

Abstract. The link between the shape of a two-dimensional, uniform vortex and self-induced velocities on its boundary is investigated through a contour-dynamics approach. The tangent derivative of the velocity along the boundary is written in a complex form, which depends on the analytic continuation of the tangent unit vector outside the vortex boundary. In this way, a classical analysis in terms of Schwarz's function of the boundary, due to Saffman, is extended to vortices of arbitrary shape. Time evolution of intrinsic quantities (tangent unit vector, curvature and Fourier's coefficients for the vortex shape) is also analyzed, showing that it depends on tangent derivatives of the velocities, only. Furthermore, a spectral method is proposed, aimed at investigating the dynamics of nearly-circular vortices in an inviscid, isochoric fluid. Comparisons with direct numerical simulations are also established.

Key words: complex analysis, contour dynamics, intrinsic dynamics of a plane curve, spectral methods, two-dimensional vorticity dynamics

1. Introduction

The study of the relation between the *shape* of a two-dimensional, uniform vortex and the corresponding *self-induced velocities* is a quite old issue of vortex dynamics. Early works date back to Kirchhoff, who found that the boundary of an elliptical vortex rotates without changing its shape [1, Art. 159].

During the eighties, this rather relevant finding led to two slightly different models for the vortex dynamics, namely the *moment model* [2] and the *elliptical model* [3], the latter appearing as a refinement of the former. Both models assume the vortices to be of elliptical shape, in order to use the above Kirchhoff solution for self-induced contributions. They possess the key-mechanism of merging, mimicking Euler's equations (see [4] and [5], for symmetric and asymmetric interactions, respectively). This is the main reason for their popularity.

In the same years, the *contour dynamics* approach (see [6], for a comprehensive discussion) became a rather powerful tool for the numerical integration of the motion of uniform vortices in an inviscid, isochoric fluid. In this approach [7], the Biot-Savart integral on the *inside* of the vortex is reduced to a line integral *along* the vortex boundary, by using Green's theorem. So, the velocity $\boldsymbol{u}$ (bold symbols indicate vectors, or complex numbers) induced by a uniform vortex P on a point $\boldsymbol{x} = x_1 + \mathrm{i}x_2$ (i is the imaginary unit) is written as:

$$\boldsymbol{u}(\boldsymbol{x}) = -\int_{\partial P} \mathrm{d}\boldsymbol{y}\; G(\boldsymbol{x} - \boldsymbol{y}), \tag{1}$$

for a unitary vorticity level. In Equation (1), ∂P is the vortex boundary and $G(\boldsymbol{x}) = 1/(2\pi)\log|\boldsymbol{x}|$ (for more details, see Section 2). One of the most appealing properties of contour

dynamics is its capability to follows small-scale motions, through a redistribution of the nodes or also a surgery of excessively thin filaments.

Some years later, contour dynamics was reconsidered from a more theoretical point of view, leading to the *conformal dynamics* [8] for vortices not too deformed with respect to a given (elliptical) shape. The bases of such an approach are due to Jimenez [9] and to Saffman [10, Section 9.2], who used the Schwarz function $\boldsymbol{\Phi}$ of the contour ∂P (if $\boldsymbol{x}$ lies on ∂P: $\boldsymbol{\Phi}(\boldsymbol{x}) = \overline{\boldsymbol{x}}$, where an overbar means complex conjugate) and a conformal mapping, in order to write suitable evolution equations. Recently, these ideas have been also successfully reconsidered by Crowdy, who found classes of steady multipolar vortical structures with line vortices inside [11] and outside [12] a central, uniform one. Such classes of stationary solutions of Euler's equations appear to be closely related to multipolar equilibria observed in high Reynolds number flows.

In the present paper, an attempt to make a contribution to the understanding of the relation between shape and self-induced velocities is performed. The analysis is based on a rather unusual way of considering the velocity (1), which works when ∂P is a sufficiently smooth curve. As a matter of fact, by considering the velocity (1) along the vortex boundary, it is crucially observed (see Section 5) that its tangent derivative depends on the analytic continuation of the function $\boldsymbol{\phi} = 1/\boldsymbol{\tau}^2$ outside the boundary itself, $\boldsymbol{\tau}$ being the tangent unit vector. In the light of Saffman's analysis, such a result is not surprising: $\boldsymbol{\phi}$ is just $\partial_{\boldsymbol{x}} \boldsymbol{\Phi}$, *i.e.*, the tangent derivative of the Schwarz function. Nevertheless, the obtained relation between vortex geometry and kinematics turns out to be very useful. The present approach can be adopted for an arbitrary vortex shape, overcoming the need of a conformal mapping [10]. Furthermore, for a particular kind of uniform vortices (considered also in Saffman's book) which are "*nearly circular*" (see Section 5, for a quantitative definition), the present approach enables us to write the self-induced boundary velocities in terms of the vorticity moments.

Additional motivations to investigate the tangent derivative of the velocity (1) stems from the time behaviour of *local* and *global* quantities related to ∂P. With regard to the former, in Section 3 the *tangent unit vector* and the *curvature* are examined, by showing that their time derivative depends on tangent velocity derivatives only. Concerning the description of the vortex as a whole, the shape of P is represented in terms of the *Fourier series* of the position $\boldsymbol{x}(s)$ on the vortex boundary, considered as a function of the curvilinear abscissa s. In Section 4, the time derivative of the related Fourier coefficients is considered. It is found that it depends on the tangent derivative of the velocity only.

The present approach allows also to evaluate analytically the tangent derivative of the velocity, as shown in Section 6 for Kirchhoff's vortex and for a simple class of multipolar vortices. Finally, among many others possible applications (*e.g.*, the extension of the moment model to non-elliptical vortices), a spectral approach to the dynamics of "*nearly circular*" vortices is developed and tested in Section 7.

2. The contour-dynamics technique

In the present paper, the relation between shape of a uniform vortex P (P being a bounded domain, having smooth and finite-length boundary, *patch* hereafter) and self-induced velocities along its boundary is investigated by using the velocity (1). Intermediate steps are verified through a contour-dynamics algorithm, which is briefly described below.

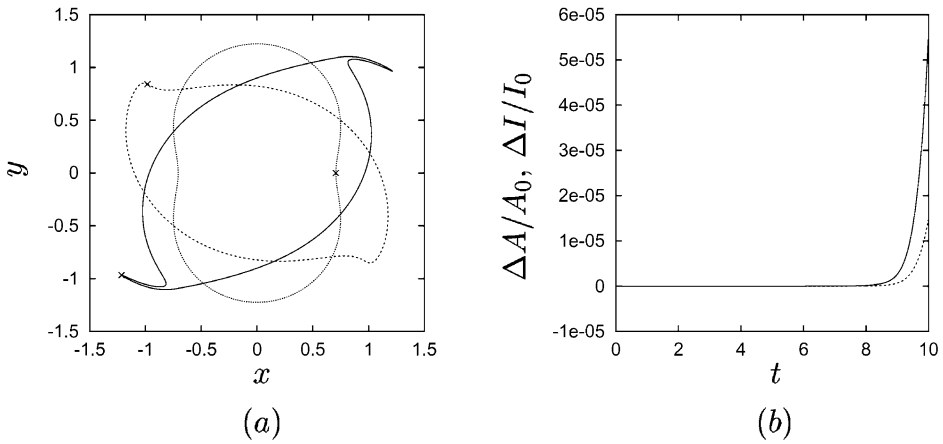

Figure 1. In (*a*), three times (0: dotted line, 5: dashed and 10: solid) of a contour dynamics simulation for a patch of kind (28), with $n = 2$ and $\varepsilon = 0{\cdot}5$, are shown. The crosses indicate the corresponding positions of the origin of the arc lengths. The time step of integration is 0·01, with a fourth order Runge-Kutta method, while $N = 200$ is assumed. In (*b*) the corresponding relative errors $(A - A_0)/A_0$ (dashed line) and $(I - I_0)/I_0$ (solid) are drawn. Note the abrupt growth of such errors at the beginning of the filamentation.

The vortex boundary at time t is represented in terms of the function $\boldsymbol{x} = \boldsymbol{x}(\sigma, t)$, where σ is a parameter (not having, in general, a Lagrangian meaning) belonging to the interval $[0, \Sigma)$. By considering the velocity (1) along ∂P, the integro-differential problem for the patch motion follows:

$$\begin{cases} \dot{\boldsymbol{x}}(\sigma, t) \;=\; -\displaystyle\int_0^{\Sigma} \mathrm{d}\sigma' \; \partial_{\sigma'} \boldsymbol{x}(\sigma', t) \; G[\boldsymbol{x}(\sigma, t) - \boldsymbol{x}(\sigma', t)] \\ \boldsymbol{x}(\sigma, 0) \qquad \text{given,} \end{cases}$$

where the dot indicates the time derivative. Recent theoretical results (see [13, Section 8.3] for a comprehensive discussion), about existence, uniqueness and global regularity of the solution of the above problem, prove that an initially smooth vortex boundary stays smooth for all times.

The form (1) of the Biot-Savart law is especially useful from a numerical point of view: the motion of the patch P is approximated by following N points $\boldsymbol{x}_q$, for $q = 1, \ldots, N$, on ∂P and by using interpolation formulae to rebuild each arc. For example, the p-th arc at the time t, *i.e.*, the portion of $\partial P(t)$ between $x_p(t)$ and $x_{p+1}(t)$, is approximated in terms of the function $\boldsymbol{x} = \boldsymbol{\Xi}_p(\sigma, t)$ for $\sigma \in (0, h)$, h being a positive number, with $\boldsymbol{\Xi}_p(0, t) = \boldsymbol{x}_p(t)$ and $\boldsymbol{\Xi}_p(h, t) = \boldsymbol{x}_{p+1}(t)$. In the present paper, a cubic interpolation law $\boldsymbol{\Xi}_p(\sigma, t) = \boldsymbol{a}(t)\,\sigma^3 + \boldsymbol{b}(t)\,\sigma^2 + \boldsymbol{c}(t)\,\sigma + \boldsymbol{d}(t)$ is employed, where the complex coefficients $\boldsymbol{a}$, $\boldsymbol{b}$, $\boldsymbol{c}$ and $\boldsymbol{d}$ are calculated by imposing also the continuity of the tangent vector, evaluated with centered fourth order derivatives, in $\boldsymbol{x}_p$ and in $\boldsymbol{x}_{p+1}$. This explicit procedure appears to be the simplest one, among the ones giving a continuous tangent vector on ∂P. The vortex motion is then approximated through a numerical integration of the system:

$$\begin{cases} \dot{\boldsymbol{x}}_q(t) \simeq -\displaystyle\sum_{p=1}^{N} \int_0^{h} \mathrm{d}\sigma \; \partial_\sigma \boldsymbol{\Xi}_p(\sigma, t) \; G[\boldsymbol{x}_q(t) - \boldsymbol{\Xi}_p(\sigma, t)] \\ \boldsymbol{x}_q(0) \qquad \text{given,} \end{cases} \tag{2}$$

for $q = 1, \ldots, N$. The number N of the points may be dynamically adjusted during a calculation and excessively thin filaments may be cut. For the sake of simplicity, none of the aforementioned procedures is adopted.

The velocity of the q-th point in Equation (2) is the sum of N terms, which are evaluated analytically. According to Pullin [14], in order to calculate the velocity induced in a point $\boldsymbol{x}$ by the p-th arc, the following relation is employed:

$$\int_0^h \mathrm{d}\sigma\ \partial_\sigma \boldsymbol{\Xi}_p\ \log|\boldsymbol{\Xi}_p - \boldsymbol{x}|^2 = (\boldsymbol{x}_{p+1} - \boldsymbol{x})\ \log|\boldsymbol{x}_{p+1} - \boldsymbol{x}|^2 - (\boldsymbol{x}_p - \boldsymbol{x})\ \log|\boldsymbol{x}_p - \boldsymbol{x}|^2 + \\ - (\boldsymbol{x}_{p+1} - \boldsymbol{x}_p) - \int_0^h \mathrm{d}\sigma\ \partial_\sigma \overline{\boldsymbol{\Xi}}_p\ \frac{\boldsymbol{\Xi}_p - \boldsymbol{x}}{\overline{\boldsymbol{\Xi}}_p - \overline{\boldsymbol{x}}}.$$

The last integral is evaluated exactly, by calculating the three roots of the algebraic equation in σ: $\boldsymbol{\Xi}_p(\sigma) = \boldsymbol{x}$.

Finally, in order to check the accuracy of the calculation, two first integrals of the motion are computed during the time integration. They are the area A of the patch and its second order moment I:

$$I = \int_P dA(\boldsymbol{x})\ |\boldsymbol{x}|^2.$$

The first integrals are analytically evaluated on the curve approximating ∂P and the differences between their initial values (A_0, I_0) and current ones are assumed as global measures of the accuracy of the numerical integration. As a sample case, in Figure 1a three successive vortex configurations are shown, while in Figure 1b the relative errors on area and second-order moment of the patch are drawn *vs.* time.

3. Intrinsic equations for the patch boundary

The tangent derivatives of the velocity on the patch boundary play an essential role in the intrinsic dynamics of that curve, *i.e.*, in time evolution of tangent unit vector ($\boldsymbol{\tau}$) and curvature ($\mathcal{K}$) measured on *material* particles lying on ∂P. As a matter of fact, as shown below, the evolution equations for $\boldsymbol{\tau}$ and $\mathcal{K}$ can be written in terms of the first and second tangent derivatives of $\overline{\boldsymbol{u}}$.

Among the possible representations of $\partial P(t)$ at a fixed time t, two are particularly useful: the Lagrangian one, in terms of the *initial* arc length s_0: $\boldsymbol{X} = \boldsymbol{X}(s_0; t)$, and the Eulerian representation, in terms of the *actual* arc length s: $\boldsymbol{x} = \boldsymbol{x}(s; t)$. The two descriptions are connected by the Lagrangian equation relating s and s_0, $s = s(s_0, t)$. By using the Lagrangian representation in order to specify the tangent unit vector as $\boldsymbol{\tau} = \partial_s \boldsymbol{x} = \partial_{s_0} \boldsymbol{X} / \partial_{s_0} s$, its time derivative can be written as follows:

$$\dot{\boldsymbol{\tau}} = \frac{\partial_{s_0} \partial_t \boldsymbol{X}}{\partial_{s_0} s} - \boldsymbol{\tau}\ \frac{\partial_{s_0} \dot{s}}{\partial_{s_0} s} = \partial_s \boldsymbol{u} - \boldsymbol{\tau}\ \partial_s \dot{s}. \tag{3}$$

From the relations $\dot{\boldsymbol{\tau}} \cdot \boldsymbol{\tau} = 0$ and (3), by considering the complex function of s: $\boldsymbol{\tau}^2 \partial_{\boldsymbol{x}} \overline{\boldsymbol{u}} = \mathcal{R}_1 + \mathrm{i}\ \mathcal{I}_1$, one obtains:

$$\partial_s \dot{s} = \boldsymbol{\tau} \cdot \partial_s \boldsymbol{u} = \mathcal{R}_1, \tag{4}$$

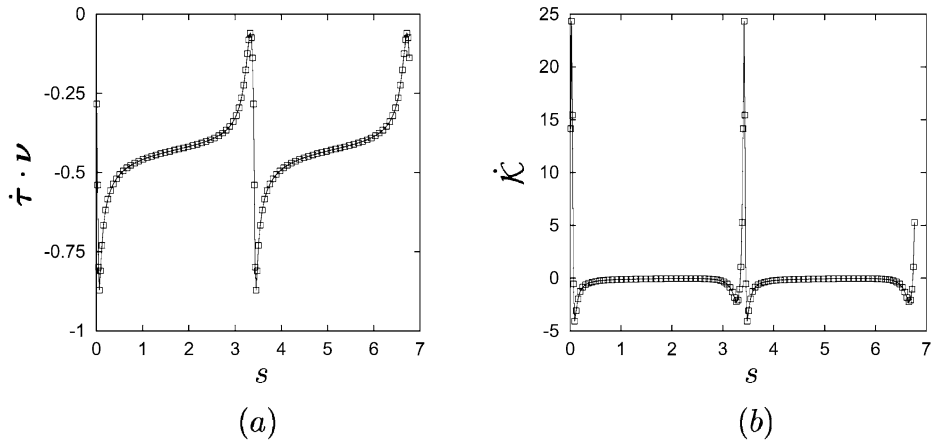

Figure 2. For the flow in Figure 1 at time 5, the normal component of $\dot{\boldsymbol{\tau}}$ (solid line) and the imaginary part ℓ_1 of $\boldsymbol{\tau}^2 \partial_{\boldsymbol{x}} \overline{\boldsymbol{u}}$ (symbols) are drawn *vs.* s in (*a*), while $\dot{\mathcal{K}}$ (solid line) and the quantity $-(3\mathcal{R}_1\mathcal{K} + \ell_2)$ (symbols) are shown in (*b*).

which implies also $\dot{\boldsymbol{\tau}} = \boldsymbol{\nu} \cdot \partial_s \boldsymbol{u}\, \boldsymbol{\nu}$, $\boldsymbol{\nu}$ being the outward normal unit vector along the patch boundary. It follows:

$$\dot{\boldsymbol{\tau}} \cdot \boldsymbol{\nu} = \ell_1, \tag{5}$$

leading also to $\dot{\boldsymbol{\tau}} = \ell_1 \boldsymbol{\nu}$ and $\dot{\boldsymbol{\nu}} = -\ell_1 \boldsymbol{\tau}$. Equation (5) is the first intrinsic equation of the dynamics of the patch boundary.

The second intrinsic equation is obtained by performing the time derivative of the relation $\mathcal{K} = \boldsymbol{\tau} \cdot \partial_s \boldsymbol{\nu} = -\boldsymbol{\nu} \cdot \partial_{s_0} \boldsymbol{\tau} / \partial_{s_0} s$:

$$\dot{\mathcal{K}} = -\dot{\boldsymbol{\nu}} \cdot \partial_s \boldsymbol{\tau} - \boldsymbol{\nu} \cdot \Big(\frac{\partial_{s_0} \dot{\boldsymbol{\tau}}}{\partial_{s_0} s} - \partial_s \boldsymbol{\tau}\, \frac{\partial_{s_0} \dot{s}}{\partial_{s_0} s} \Big) = -\partial_s \ell_1 - \mathcal{K}\ \boldsymbol{\tau} \cdot \partial_s \boldsymbol{u},$$

where $\boldsymbol{\tau} \cdot \partial_s \boldsymbol{u} = \mathcal{R}_1$. By considering the quantity $\boldsymbol{\tau}^3\, \partial^2_{\boldsymbol{xx}} \overline{\boldsymbol{u}} = \mathcal{R}_2 + \mathrm{i}\, \ell_2$, the above equation is rewritten as:

$$\dot{\mathcal{K}} + 3\, \mathcal{R}_1\, \mathcal{K} = -\ell_2, \tag{6}$$

which is the intrinsic equation for the curvature.

As an example, left and right sides in Equations (5, 6) are drawn *vs.* s in Figure 2, through contour dynamics simulations (derivatives in t and in σ are approximated via fourth-order centered formulae): the intrinsic equations appear to be verified, at least in the limits of the numerical approximations.

4. Time derivative of the Fourier coefficients of the patch boundary, with the natural parameterization

In the present section, a relation between the time derivative of the Fourier coefficients for the patch shape and the tangent derivative of the self-induced boundary velocities is established.

To this end, the choice of the boundary parameterization plays a crucial role. Here the arc length s is used, having the intrinsic relation (4) between the Lagrangian time derivative of s and the tangential derivative of the velocity. As a consequence, the time derivative of any

Fourier coefficient (unless the one having a vanishing wave number) can be written in terms of the self-induced velocities on the boundary only. In order to define the curvilinear abscissa in a Lagrangian way, a point $\boldsymbol{x}_0(0)$ on the vortex boundary is fixed as origin of the arc lengths, at the initial time ($t = 0$). Such a curvilinear abscissa is indicated with s_0 (see also Section 3). At later times ($t > 0$), the origin $\boldsymbol{x}_0(t)$ of the curvilinear abscissa s at the actual time t is chosen on the Lagrangian image of the initial one $\boldsymbol{x}_0(0)$, *i.e.*, on the position at time t of the particle which was in $\boldsymbol{x}_0(0)$ at time 0.

When the length of ∂P at time t is defined by $l(t)$ (with $l(0) = l_0$) and the time dependent k-th wave number by $\mathrm{K}(t) = 2k\pi/l(t)$, the k-th Fourier coefficient for the patch boundary may be written as:

$$\boldsymbol{c}_k(t) = \frac{1}{l(t)} \int_0^{l(t)} \mathrm{d}s \; \boldsymbol{x}(s,t) \; \exp\left[-\mathrm{i}\,\mathrm{K}(t)\, s\right] \tag{7}$$

and the position $\boldsymbol{x}(s,t)$ of the point on the curve ∂P, placed at a curvilinear abscissa s at time t, is given by the Fourier series:

$$\boldsymbol{x}(s,t) = \sum_k \boldsymbol{c}_k(t) \; \exp\left[\,\mathrm{i}\,\mathrm{K}(t)\, s\,\right] \tag{8}$$

(hereafter, if the extremes of the sum are not indicated, they are $-\infty$ and $+\infty$, respectively). It is worth noticing that, at least for $k \neq 0$, the Fourier coefficients (7) do not depend *on the position* of the arc length origin $\boldsymbol{x}_0$, because they may be written as:

$$\boldsymbol{c}_k = \frac{1}{k} \frac{1}{2\pi\mathrm{i}} \int_0^{l} \mathrm{d}s \; \boldsymbol{\tau} \; \exp\left(-\mathrm{i}\,\mathrm{K}\, s\,\right).$$

On the contrary, $\boldsymbol{c}_0$ may be given as follows:

$$\boldsymbol{c}_0 = \boldsymbol{x}_0 - \frac{1}{l} \int_0^{l} \mathrm{d}s \; \boldsymbol{\tau} \; s,$$

i.e., as sum of the position $\boldsymbol{x}_0$ and of an intrinsic part. Obviously, the Fourier coefficients depend *on the choice* of the point $\boldsymbol{x}_0(0)$ along the initial curve $\partial P(0)$.

By using the map $s = s(s_0, t)$, the k-th coefficient is rewritten in the following Lagrangian form:

$$\boldsymbol{c}_k(t) = \frac{1}{l(t)} \int_0^{l_0} \mathrm{d}s_0 \underbrace{\partial_{s_0} s(s_0,t)}_{\substack{\text{Jacobian of the} \\ \text{transformation}}} \underbrace{\boldsymbol{x}[s(s_0,t),t]}_{\substack{\text{Lagrangian} \\ \text{position}}} \underbrace{\exp\left[-\mathrm{i}\,\mathrm{K}(t)\, s(s_0,t)\,\right]}_{\substack{\text{exponential in} \\ \text{Lagrangian form}}},$$

where the derivative $\partial_{s_0} s$ is positive, due to the regularity of the Lagrangian map and the initial condition $s(s_0, 0) = s_0$. By taking the time derivative of the k-th Fourier coefficient $\boldsymbol{c}_k$, written in the above Lagrangian form, the following relation is obtained:

$$\dot{\boldsymbol{c}}_k = \underbrace{\frac{1}{l} \int_0^{l} \mathrm{d}s \; \boldsymbol{u} \; e^{-\mathrm{i}\,\mathrm{K}\, s}}_{\boldsymbol{U}_k} + \underbrace{\frac{1}{l} \int_0^{l} \mathrm{d}s \; (v - \mathrm{i}\,\mathrm{K}\, w)\, \boldsymbol{x} \; \mathrm{e}^{-\mathrm{i}\,\mathrm{K}\, s}}_{\boldsymbol{X}_k}. \tag{9}$$

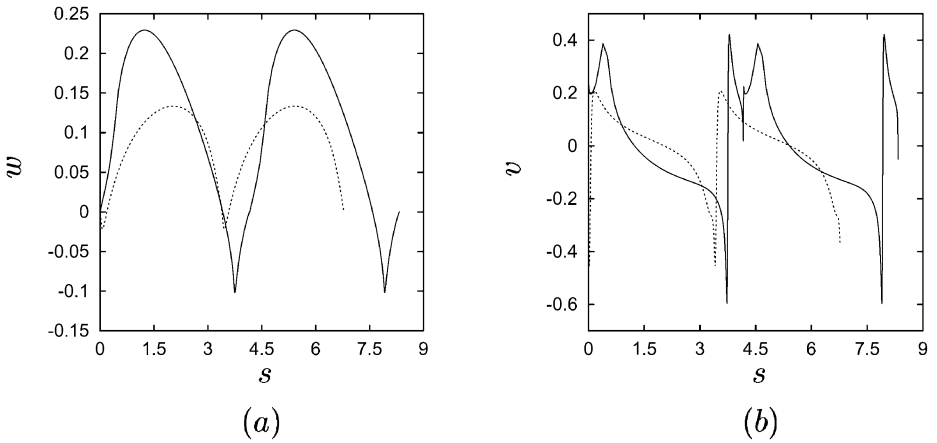

Figure 3. For the vortex motion shown in Figure 1a, the functions $w(s,t) = \dot{s}(s,t) - \Lambda s$ and $v(s,t) = \partial_s \dot{s}(s,t) - \Lambda$ at the times 5 (dashed line) and 10 (solid) are drawn *vs.* s in (*a*) and (*b*), respectively.

As to the first term $\boldsymbol{U}_k$ in the right-hand side of Equation (9), it is worth noticing that, for $k \neq 0$, an arbitrary function of time can be added to $\boldsymbol{u}$, without modifying the value of $\boldsymbol{U}_k$. In the second term $\boldsymbol{X}_k$, the real functions $w(s,t)$ and $v(s,t)$ are defined as:

$$w = \dot{s} - \Lambda s, \quad v = \partial_s w, \tag{10}$$

where $\Lambda = \dot{l}/l$ is the relative elongation velocity of the patch boundary. With regard to the functions w and v, it is worth noticing that the time derivative of l is given by:

$$\dot{l} = \int_0^{l_0} \mathrm{d}s_0 \; \partial_{s_0} \dot{s} = \int_0^{l} \mathrm{d}s \; \partial_s \dot{s} = \dot{s}(l), \tag{11}$$

with $\dot{s}(0) = 0$, by the definition of the origin of the arc length s. It follows that $w(0) = w(l) = 0$, so w and, as a consequence, v are continuous periodic functions of s, despite the jump of $\dot{s}(s)$ in passing from $s = l$ to $s = 0$. In Figure 3, the functions w and v are drawn *vs.* s at two times of the contour dynamics simulation of Figure 1. Note also that the relative elongation velocity Λ is just the mean value of the function $\partial_s \dot{s}(s)$, so that v has a vanishing mean (its Fourier coefficient $\boldsymbol{v}_0$ vanishes); see Figure 3b.

The whole right-hand side of Equation (9) may be rewritten in terms of the Fourier coefficients for the position $\boldsymbol{x}$ and the tangent derivative $\partial_{\boldsymbol{x}} \overline{\boldsymbol{u}}$. Actually, the term $\boldsymbol{U}_k$ may be easily rewritten for $k = 0$:

$$\boldsymbol{U}_0 = \dot{\boldsymbol{x}}_0 - \frac{1}{l} \int_0^{l} \mathrm{d}s \; s \; \partial_s \boldsymbol{u}, \tag{12}$$

where $\dot{\boldsymbol{x}}_0$ is the velocity of $\boldsymbol{x}_0$. Otherwise, when $k \neq 0$, it may be rewritten as:

$$\boldsymbol{U}_k = -\frac{\mathrm{i}}{\mathrm{K}} \frac{1}{l} \int_0^{l} \mathrm{d}s \; \partial_s \boldsymbol{u} \; \mathrm{e}^{-\mathrm{i}\,\mathrm{K}\,s}. \tag{13}$$

Finally, in the term $\boldsymbol{X}_k$ in Equation (9), the integral in w may be rewritten as one in v, by using the identity:

$$\boldsymbol{x} \; \mathrm{e}^{-\mathrm{i}\mathrm{K}s} \equiv \partial_s \left[\boldsymbol{c}_k \; s - \mathrm{i} \sum_{m \neq k} \frac{\boldsymbol{c}_m}{\mathrm{M} - \mathrm{K}} \; \mathrm{e}^{\mathrm{i}\,(\mathrm{M}-\mathrm{K})\,s} \right], \tag{14}$$

so Equation (4) leads to a form in which only the tangent velocity derivative appears. The resulting spectral formulation for the patch dynamics will be presented in Section 7, under simplifying assumptions on the patch shape, at the present time. In particular, the relation between vortex shape and tangent derivative of the self-induced velocity will be established through the following coefficients:

$$\boldsymbol{e}_{k,m} = \frac{1}{l} \int_0^l \mathrm{d}s \; \frac{\mathrm{e}^{-\mathrm{i}\,\mathrm{K}\,s}}{(\boldsymbol{x} - \boldsymbol{\alpha})^m}, \tag{15}$$

$\boldsymbol{\alpha}$ being a suitable, fixed point within the vortex. It will be shown that only the coefficients (15) for $m = 1$ are needed, the other coefficients ($\boldsymbol{e}_{k,m}$ for $m > 1$) being deduced from the ones $\boldsymbol{e}_{k,1}$, via suitable recurrence formulae. However, also these coefficients are functions of the time, through the length l, the position $\boldsymbol{x}$ and the arc length s. So, they must be integrated in time, together with the Fourier coefficients (7) of the patch shape. To this end, the time derivative of the coefficient $\boldsymbol{e}_{m,1}$ is evaluated as:

$$\dot{\boldsymbol{e}}_{m,1} = \frac{1}{l} \int_0^l \mathrm{d}s \; \frac{\mathrm{e}^{-\mathrm{i}\,\mathrm{M}\,s}}{\boldsymbol{x} - \boldsymbol{\alpha}} \left(v - \mathrm{i}\,\mathrm{M}\; w - \frac{\boldsymbol{u}}{\boldsymbol{x} - \boldsymbol{\alpha}} \right), \tag{16}$$

which will be discussed in Section 7.

The importance of the tangent derivative of the self-induced velocity on the patch boundary has been established, both from a *local* point of view (time derivative of tangent unit vector and curvature, see Section 3) and from a *global* one (time derivative of the Fourier coefficients for the patch shape). An easy and useful form of such a derivative is deduced in the next section.

5. Derivative of the velocity along the vortex boundary

The velocity field induced by a patch of unit vorticity is considered in the contour dynamics form (1), which holds throughout the plane, including the patch boundary. In the present section, the derivative with respect to the curvilinear abscissa s of the self-induced velocity $\boldsymbol{u}(s) = \boldsymbol{u}[\boldsymbol{x}(s)]$ on the patch boundary is considered.

In a point $\boldsymbol{x}$ on ∂P, in which the curve is sufficiently smooth,[1] the derivative of the velocity (1) with respect to s is given by:

$$\partial_s \boldsymbol{u}\,[\boldsymbol{x}(s)] = -\frac{1}{2\pi} \fint_{\partial P} \mathrm{d}\boldsymbol{y} \; \frac{\boldsymbol{x}(s) - \boldsymbol{y}}{|\boldsymbol{x}(s) - \boldsymbol{y}|^2} \cdot \boldsymbol{\tau}(s), \tag{17}$$

where the Cauchy principal value of the integral is considered and the dot indicates a scalar product. By introducing the function $\boldsymbol{\phi} = 1/\boldsymbol{\tau}^2$, Equation (17) is rewritten in the following complex form:

$$\partial_{\boldsymbol{x}} \overline{\boldsymbol{u}}(\boldsymbol{x}) = -\frac{\mathrm{i}}{2} \left[\frac{1}{2\pi\,\mathrm{i}} \fint_{\partial P} \mathrm{d}\boldsymbol{y} \; \frac{\boldsymbol{\phi}(\boldsymbol{y})}{\boldsymbol{x} - \boldsymbol{y}} + \frac{1}{2}\, \boldsymbol{\phi}(\boldsymbol{x}) \right] = -\frac{\mathrm{i}}{2}\, \boldsymbol{V}(\boldsymbol{x}). \tag{18}$$

The function $\boldsymbol{V}(\boldsymbol{x})$ in the square brackets can be evaluated by standard tools of complex analysis, if the analytical continuation of the function $\boldsymbol{\phi}$ is known in a suitable portion of the complex plane. A useful form of that term is obtained by considering the closed curve[2]

[1] A proof (by the author) for a curve ∂P having continuous third derivative is also available, on request.

[2] The set $\partial P_r(\boldsymbol{x})$ may be defined also as ∂P, unless a small circular neighbourhood $B_r(\boldsymbol{x})$ of the point $\boldsymbol{x}$ of radius r. Here, $B'_r(\boldsymbol{x})$ indicates the complementary set of $B_r(\boldsymbol{x})$.

$\partial P_r(\boldsymbol{x})$, composed by joining $\partial P \cap B'_r(\boldsymbol{x})$ and the half circle $\partial B_r^-(\boldsymbol{x})$, internal to the patch. By using this curve, $\boldsymbol{V}$ may be rewritten as:

$$\boldsymbol{V}(\boldsymbol{x}) = \frac{1}{2\pi\,\mathrm{i}} \lim_{r \to 0^+} \int_{\partial P_r(\boldsymbol{x})} \mathrm{d}\boldsymbol{y}\, \frac{\boldsymbol{\phi}(\boldsymbol{y})}{\boldsymbol{x}-\boldsymbol{y}}. \tag{19}$$

A few sample cases, in which the function $\boldsymbol{V}(\boldsymbol{x})$ is evaluated analytically, are discussed in the next section.

The result (18) is not surprising in view of Saffman's analysis [10]. As mentioned in Section 1, Saffman found a relation between self-induced velocities of the patch and the Schwarz function of its boundary, at least for "*nearly circular*" patches. This constraint on the shape is due to the use of Laurent expansions for the Schwarz function and for a conformal map between patch and unit circle, which are assumed possible on the vortex boundary. The connection between Saffman's analysis and the present one lies in the following relation:

$$\boldsymbol{\phi} = \frac{\overline{\boldsymbol{\tau}}}{\boldsymbol{\tau}} = \partial_{\boldsymbol{x}} \overline{\boldsymbol{x}} = \partial_{\boldsymbol{x}} \boldsymbol{\Phi}, \tag{20}$$

which states that the function $\boldsymbol{\phi}$ is just the tangent derivative of the Schwarz function $\boldsymbol{\Phi}$ of the vortex boundary. In author's opinion, the present rereading of Saffman's analysis extends it to patches of arbitrary shape. Moreover, also for the "*nearly circular*" patches considered below, the current approach leads to an improvement, by relating in a direct manner *self-induced velocities* and *moments* of a patch. This clears the way for a new kind of moment model, working with "*nearly circular*" vortices, which overcomes the difficulties due to self-induced effects, without assuming elliptical shapes.

Consider a particular class of vortices, having the function $\boldsymbol{\phi}$ which can be written as a Laurent series in an annular region with center in a point $\boldsymbol{\alpha}$ (within the vortex) and including the vortex boundary ∂P. A patch of this kind will be defined as "*nearly circular*" hereafter. In this case, the relation between vortex shape ($\boldsymbol{\phi}$) and tangent derivative of the velocity ($\partial_{\boldsymbol{x}} \overline{\boldsymbol{u}}$) is thoroughly clarified by considering that the function $\boldsymbol{V}$ (18) may be decomposed as:

$$\boldsymbol{V} = \boldsymbol{\phi} - \boldsymbol{\psi}, \tag{21}$$

where the function $\boldsymbol{\psi}$ is defined as follows:

$$\boldsymbol{\psi}(\boldsymbol{x}) = -\frac{1}{2\pi\,\mathrm{i}} \int_{\partial P} \mathrm{d}\boldsymbol{y}\, \frac{\boldsymbol{\phi}(\boldsymbol{y})}{\boldsymbol{x}-\boldsymbol{y}} + \frac{1}{2}\,\boldsymbol{\phi}(\boldsymbol{x}). \tag{22}$$

If the function $\boldsymbol{\phi}$ can written as a Laurent series on ∂P, the corresponding expansion in a power series of $\boldsymbol{x}-\boldsymbol{\alpha}$ of the function $\boldsymbol{\psi}$ follows from its definition (22). As a matter of fact, by considering a term of the kind $\boldsymbol{\phi} \sim (\boldsymbol{x}-\boldsymbol{\alpha})^k$, with k positive, in the Laurent series for $\boldsymbol{\phi}$, the corresponding term in the expansion for $\boldsymbol{\psi}$ is given by:

$$\boldsymbol{\psi}(\boldsymbol{x}) \sim -\frac{1}{2\pi\;\mathrm{i}}\,(\boldsymbol{x}-\boldsymbol{\alpha})^k \int_{\partial P} \frac{\mathrm{d}\boldsymbol{y}}{\boldsymbol{x}-\boldsymbol{y}} + \frac{1}{2}\,(\boldsymbol{x}-\boldsymbol{\alpha})^k \sim \boldsymbol{\phi}(\boldsymbol{x}),$$

i.e., the coefficients of the term in $(\boldsymbol{x}-\boldsymbol{\alpha})^k$ in the power series for $\boldsymbol{\phi}$ and $\boldsymbol{\psi}$ are equal. On the contrary, any term with k negative in the Laurent series for $\boldsymbol{\phi}$ gives a vanishing contribution to the function $\boldsymbol{\psi}$. To show this fact, the term $\boldsymbol{\phi}(\boldsymbol{x}) \sim (\boldsymbol{x}-\boldsymbol{\alpha})^{-k'}$ for k' positive of the Laurent series for the function $\boldsymbol{\phi}$ is considered. By using the identity:

$$\begin{aligned}\frac{1}{(\boldsymbol{y}-\boldsymbol{\alpha})^{k'}\,(\boldsymbol{x}-\boldsymbol{y})} \;\equiv\; & \frac{1}{(\boldsymbol{x}-\boldsymbol{\alpha})^{k'}}\left(\frac{1}{\boldsymbol{x}-\boldsymbol{y}} + \frac{1}{\boldsymbol{y}-\boldsymbol{\alpha}}\right) + \\ & + \frac{\boldsymbol{b}_2}{(\boldsymbol{y}-\boldsymbol{\alpha})^2} + \ldots + \frac{\boldsymbol{b}_{k'}}{(\boldsymbol{y}-\boldsymbol{\alpha})^{k'}},\end{aligned}$$

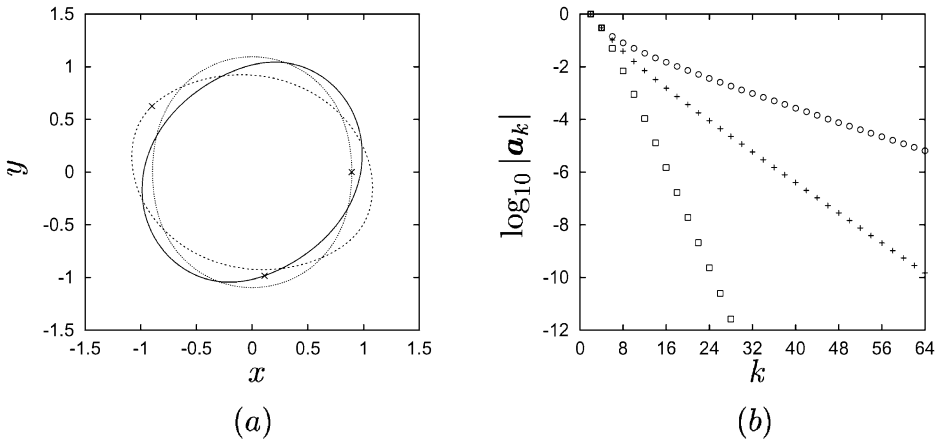

Figure 4. Sample of vortex dynamics for a patch of kind (28), with $n = 2$ and $\varepsilon = 0{\cdot}2$: in (*a*) the patch geometries at times 0 (dotted line), 5 (dashed) and 10 (solid) are shown (the crosses indicate the positions of the point $\boldsymbol{x}_0$, origin of the arc lengths), while in (*b*) the logarithm of the modulus of the Laurent coefficients $\boldsymbol{a}_k$ (24) at times 0 (squares), 5 (circles) and 10 (crosses) is drawn *vs.* k.

where the quantities $\boldsymbol{b}_p$ for $p = 2, 3, \ldots, k'$ do not depend on $\boldsymbol{y}$, the corresponding contribution to the function $\boldsymbol{\psi}$ results:

$$\boldsymbol{\psi}(\boldsymbol{x}) \sim -\frac{1}{2\pi\,\mathrm{i}}\,\frac{1}{(\boldsymbol{x}-\boldsymbol{\alpha})^{k'}}\left(\oint_{\partial P}\frac{\mathrm{d}\boldsymbol{y}}{\boldsymbol{x}-\boldsymbol{y}}+\int_{\partial P}\frac{\mathrm{d}\boldsymbol{y}}{\boldsymbol{y}-\boldsymbol{\alpha}}\right)+\frac{1}{2}\,\frac{1}{(\boldsymbol{x}-\boldsymbol{\alpha})^{k'}}=0.$$

In this way, from Equation (21), the following series expansion for the velocity derivative is obtained:

$$\partial_{\boldsymbol{x}}\overline{\boldsymbol{u}}(\boldsymbol{x}) = -\frac{\mathrm{i}}{2}\sum_{k=2}^{+\infty}\frac{\boldsymbol{a}_k}{(\boldsymbol{x}-\boldsymbol{\alpha})^k} = -\frac{1}{2\pi\,\mathrm{i}}\sum_{k=0}^{+\infty}\frac{(k+1)\boldsymbol{M}_k}{(\boldsymbol{x}-\boldsymbol{\alpha})^{k+2}}, \tag{23}$$

where the k-th Laurent coefficient of the function $\boldsymbol{\phi}$ is given by:

$$\boldsymbol{a}_k = \frac{1}{2\pi\,\mathrm{i}}\int_{\partial P}\mathrm{d}\boldsymbol{x}\;(\boldsymbol{x}-\boldsymbol{\alpha})^{k-1}\,\boldsymbol{\phi}(\boldsymbol{x}) = -\frac{k-1}{\pi}\,\boldsymbol{M}_{k-2} \tag{24}$$

and $\boldsymbol{M}_k$ is the k-th moment of the patch [2] with respect to the point $\boldsymbol{\alpha}$:

$$\boldsymbol{M}_k = \int_P \mathrm{d}A(\boldsymbol{x})(\boldsymbol{x}-\boldsymbol{\alpha})^k = \frac{\mathrm{i}}{2}\,\frac{1}{k+1}\int_{\partial P}\mathrm{d}\boldsymbol{x}\;(\boldsymbol{x}-\boldsymbol{\alpha})^{k+1}\boldsymbol{\phi}(\boldsymbol{x}).$$

Equation (23) shows that the tangent derivative of the conjugate of the velocity is given by the singular part (times $-\mathrm{i}/2$) of the Laurent series for $\boldsymbol{\phi}$ or, through the relation (24), by a moment expansion. Moreover, it holds on ∂P and outside it, but not within that curve, the derivative of $\overline{\boldsymbol{u}}$ not being continuous across the patch boundary. Finally, by assuming that at infinity the fluid is at rest, first and last sides in Equation (23) may be integrated, to obtain:

$$\overline{\boldsymbol{u}}(\boldsymbol{x}) = \frac{1}{2\pi\,\mathrm{i}}\sum_{k=0}^{+\infty}\frac{\boldsymbol{M}_k}{(\boldsymbol{x}-\boldsymbol{\alpha})^{k+1}}, \tag{25}$$

which holds on ∂P and outside it. From the above relation, a direct connection between boundary velocities and moments is established, showing also the considerable simplicity

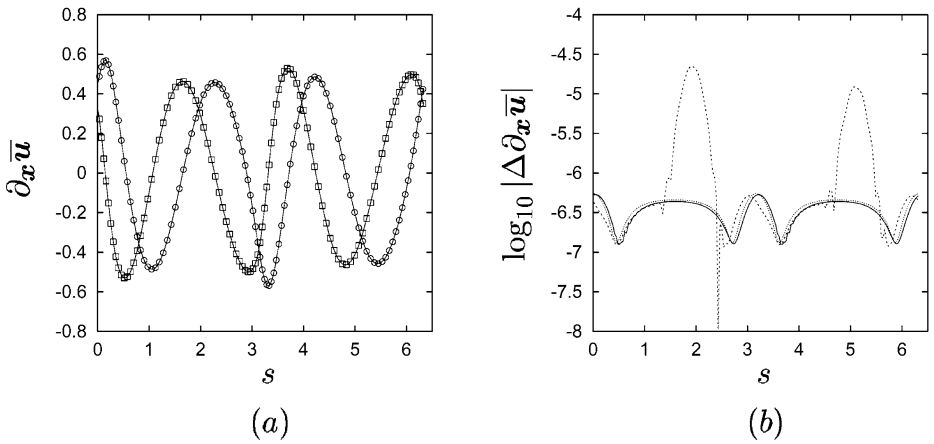

Figure 5. In (*a*) are drawn the tangential (squares) and normal (circles) components of the tangent derivative $\partial_{\boldsymbol{x}}\overline{\boldsymbol{u}}$ *vs.* the arc length s, for the flow in Figure 4 at time 5. The components are evaluated numerically (solid line), through the contour-dynamics velocity (1), and analytically (symbols), by using the series (23) with 120 terms. In (*b*) the logarithm of the difference between numerical and analytical tangent derivatives, at times 0 (dotted line), 5 (dashed) and 10 (solid), is drawn *vs. s*.

of such patches. Equation (25) is just the starting point to build a moment model for nearly circular patches, with exact self-induced effects. This issue is actually under investigation.

An example of the calculation of the coefficients (24) is given in Figure 4, which shows the differences in the convergence rates of the series (23) at three times, during the motion of a given, nearly circular patch. A comparison between the tangent derivative of the velocity given by a numerical evaluation (with a fourth-order centered scheme) of the contour dynamics velocity (1) and by the series (23) is carried out in Figure 5. Even if the effects of each source of numerical errors (curve interpolation, discrete derivatives and integrals) cannot be easily understood, a satisfactory agreement between the two tangent derivatives appears to be reached.

6. Sample cases

In this section few sample cases, in which the limit (19) may be analytically evaluated, are briefly discussed. The function $\boldsymbol{\phi}$ is found everywhere in the complex plane and its singularities lead to the estimate of the above limit, through the Cauchy or the residue theorems. The aim of the present calculations is the study of the singularities of the function $\boldsymbol{\phi}$, for rather non-trivial patch shapes. This analysis must be understood as a preliminary step in order to investigate, in a future work, the time evolution of such singularities. For the reader's convenience, technical details are summarized in Appendix A.

6.1. The elliptical patch

The unitary vorticity is spread on an ellipse, having semi-axes of lengths a (along the real axis x) and b (along the imaginary axis y), with $a > b$. The aspect ratio $\lambda = a/b$ will be also used.

The boundary of the vortex is defined as $\boldsymbol{x}(\theta) = a\cos\theta + \mathrm{i}b\sin\theta$, where θ runs from 0 to 2π. It follows that:

$$\mathrm{e}^{\mathrm{i}\,\theta} = z = \frac{\boldsymbol{x} + \sqrt{\boldsymbol{x}^2 - c^2}}{a+b} = \frac{1}{a}\,(x + \mathrm{i}\,\lambda\,y), \tag{26}$$

where $c = \sqrt{a^2 - b^2}$ is one half focal length. The relation (26) maps the patch boundary in the unit circle $\partial\mathcal{C}$. The function $\boldsymbol{\phi}$ is given as:

$$\boldsymbol{\phi} = \frac{\gamma^2 z^2 - 1}{z^2 - \gamma^2} = \frac{1}{\lambda^2 - 1}\left[(\lambda^2+1) - 2\lambda\,\frac{\boldsymbol{x}}{\sqrt{\boldsymbol{x}^2 - c^2}}\right], \tag{27}$$

in the transformed z-plane and in the physical one, with $\gamma^2 = (\lambda-1)/(\lambda+1) < 1$. In the first plane, $\boldsymbol{\phi}$ turns out to be singular on the two poles $\pm\gamma$, while in the second $\boldsymbol{\phi}$ is discontinuous on the segment joining the two foci of the ellipse, which are branch points for the square root. As shown in Equation (A1) of the Appendix A, the tangent derivative of the boundary velocity follows, through Equation (19), as:

$$\partial_{\boldsymbol{x}}\overline{\boldsymbol{u}} = \frac{2\,\mathrm{i}\,\lambda}{\lambda+1}\,\frac{1}{(\lambda+1)z^2 - (\lambda-1)} = \frac{\mathrm{i}\,a\,b}{\boldsymbol{x}^2 - \boldsymbol{c}^2 - \boldsymbol{x}\,\sqrt{\boldsymbol{x}^2 - \boldsymbol{c}^2}},$$

which may be also integrated, leading to the definition of $\boldsymbol{u}$ on the vortex boundary. Actually, by considering that

$$\partial_z \boldsymbol{x} = \frac{a}{2\lambda}\,\frac{(\lambda+1)z^2 - (\lambda-1)}{z^2},$$

the z-derivative of the tangent velocity field is written as:

$$\partial_z\overline{\boldsymbol{u}} = \mathrm{i}\,\frac{a}{\lambda+1}\,\frac{1}{z^2}.$$

By accounting for the map (26), the integration in z of the above relation gives the boundary velocity:

$$\boldsymbol{u}(\boldsymbol{x}) = \frac{\mathrm{i}}{\lambda+1}\,(x + \mathrm{i}\,\lambda\,y),$$

which is Kirchhoff's solution.

6.2. A CLASS OF MULTIPOLAR PATCHES

As other sample cases, the tangent derivative of the velocity is analytically evaluated for a contrived class of patches, each of them having a boundary defined in the following way:

$$\boldsymbol{x}(\theta) = \rho(\theta)\,\mathrm{e}^{\mathrm{i}\,\theta}, \quad \text{with:} \quad \rho(\theta) = (1 - \varepsilon\cos n\theta)^{1/n}, \tag{28}$$

where n is a positive integer, $\theta \in [0, 2\pi)$ and ε is a real parameter, with $0 < \varepsilon < 1$, which controls the deepness of the perturbation of the circular shape ($\varepsilon = 0$). Furthermore, related quantities $\mu = [(1-\varepsilon^2)/(2\varepsilon)]^{1/n}$ and $\delta = (\varepsilon/2)^{1/n}$ are also used below.

By following the general approach described in Appendix 9, the boundary velocity for the patch with $n = 1$ (which is nearly circular for any ε and $\boldsymbol{\alpha} = -\delta$) is given by:

$$\overline{\boldsymbol{u}}(\boldsymbol{x}) = \frac{1}{2\pi\,\mathrm{i}}\left[\frac{2+\varepsilon^2}{2}\,\pi\,\frac{1}{\boldsymbol{x}+\delta} - \frac{\pi\varepsilon}{2}\,\frac{1}{(\boldsymbol{x}+\delta)^2}\right]$$

where $(2+\varepsilon^2)\pi/2 = \boldsymbol{M}_0$ is just the area of the patch and $-\pi\varepsilon/2 = \boldsymbol{M}_1$, while $\boldsymbol{M}_k = 0$ for any $k \geq 2$, according to Equation (25). For $n = 2$, the boundary velocity follows as:

$$\overline{\boldsymbol{u}}(\boldsymbol{x}) = \frac{1}{2\pi i}\,\frac{\pi}{2}\left(\frac{1}{\boldsymbol{x}-\mathrm{i}\delta}+\frac{1}{\boldsymbol{x}+\mathrm{i}\delta}\right), \tag{29}$$

which is identical to the one due to a couple of point vortices having equal circulations (one half of the patch circulation π), placed on the two poles of the function $\boldsymbol{\phi}$ ($\boldsymbol{x} = \pm\,\mathrm{i}\,\delta$), inside the patch. Moreover, the patch is nearly circular for $\varepsilon < 2/3$ and $\boldsymbol{\alpha} = 0$. In this case $\boldsymbol{M}_{2k'} = \pi(-1)^{k'}\delta^{2k'}$ and $\boldsymbol{M}_{2k'+1} = 0$ for $k' = 0, 1, 2, \ldots$, so that Equation (25) leads to:

$$\overline{\boldsymbol{u}}(\boldsymbol{x}) = \frac{1}{2\pi\,\mathrm{i}}\sum_{k'=0}^{+\infty}\frac{\pi(-1)^{k'}\delta^{2k'}}{\boldsymbol{x}^{2k'+1}},$$

which may also be obtained by considering the corresponding Laurent series for the velocity (29).

The general case ($n \geq 3$) is much more complicated: details[3] about the calculations are summarized in Appendix A, where the tangent derivative of the velocity is evaluated for an arbitrary n; see Equation (A11). It appears convenient to work in the transformed plane $\boldsymbol{z} = \exp(\mathrm{i}\,\theta)$, where ∂P becomes the unit circle $\partial\mathcal{C}$ and the function $\boldsymbol{\phi}$ exhibits n branch cuts inside and n outside (up to the infinity) the curve $\partial\mathcal{C}$. A comparison between analytical and numerical tangent derivatives is shown in Figure 6 for the patches for $n = 10$ (first row) and $n = 11$ (second row). The agreement appears to be satisfactory, at least in the limit of the numerical approximations.

After having discussed a few sample cases, as applications of Equation (19) to patches of simple shape, the use of the tangent velocity derivative for the dynamics of the Fourier coefficients (7) will now be addressed.

7. Intrinsic spectral dynamics

A spectral method is used to investigate the vortex dynamics as the result of interactions between different wave-number components, related in the simple Fourier way (8) to the patch shape. As a matter of fact, even if contour dynamics remains the most appropriate and efficient approach to simulate the motion numerically, its results do not have the same direct physical meaning as the spectral ones.

In Section 4 it has been shown that the time derivative of the Fourier coefficients (7) can be written in terms of the tangential derivative of the boundary velocity only. Once the relation between $\partial_{\boldsymbol{x}}\overline{\boldsymbol{u}}$ and the vortex shape has been discussed in Section 5, it becomes possible to develop the *intrinsic spectral formulation* (see Equation (34), below), for an arbitrary shape of the vortex. However, in order to close such a system of equations, the Fourier coefficients of the tangent derivative of the velocity must be expressed in terms of the Fourier coefficients of the patch shape (7). At this stage of the study, this is done *only* for nearly circular vortices.

The tangent derivative of the boundary velocity is written in terms of the following Fourier series:

$$\boldsymbol{\tau}(s,t)\;\partial_{\boldsymbol{x}}\overline{\boldsymbol{u}}[\boldsymbol{x}(s,t)] = \partial_s\overline{\boldsymbol{u}}(s,t) = \sum_k \boldsymbol{d}_k(t)\;\mathrm{e}^{\mathrm{i}\,\mathrm{K}\,s} \tag{30}$$

[3] A detailed report (by the author) is also available, on request.

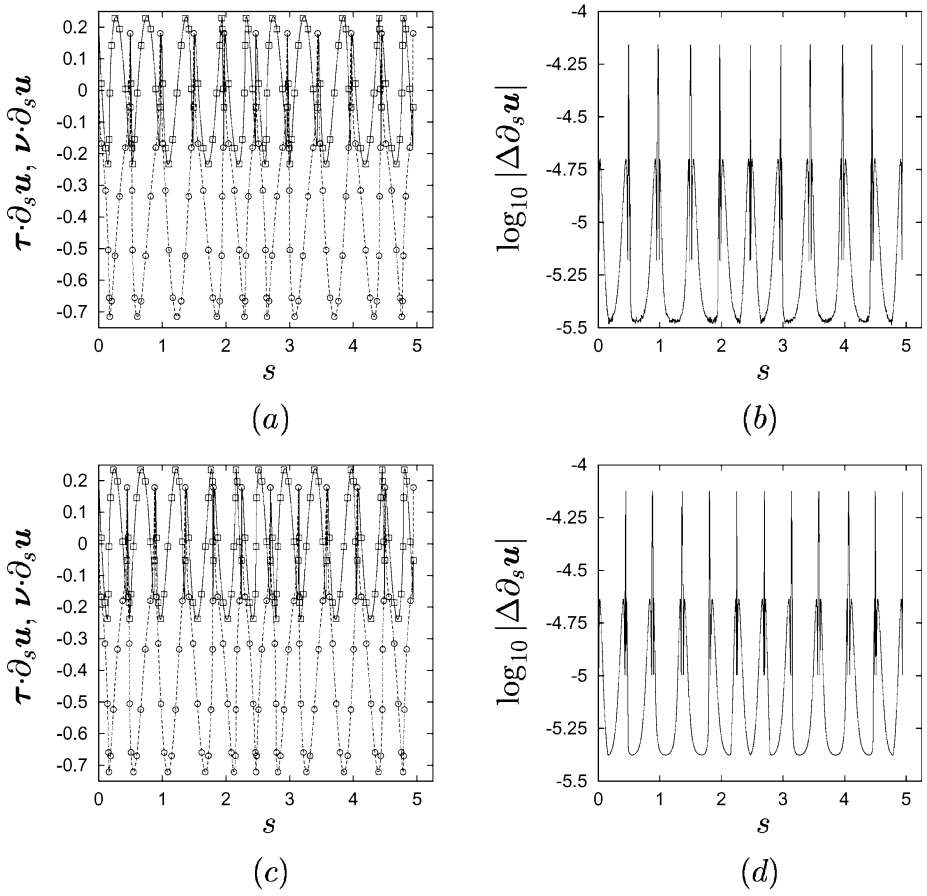

Figure 6. In the first column the tangential (analytical: solid line, numerical: squares) and normal (analytical: dashed line, numerical: circles) components of the derivative $\partial_s \boldsymbol{u}$ for a patch of kind (28) with $\varepsilon = 0{\cdot}8$ are drawn *vs. s*, while in the second column (*b*, *d*) the logarithm of the modulus of the difference between numerical ($N = 1000$ in *b*, $N = 1100$ in *d*) and analytical derivatives is drawn *vs. s*. In the first row (*a*, *b*) $n = 10$ and in the second one (*c*, *d*) $n = 11$. On each arc element, the derivatives are evaluated in $\sigma = h/2$ and, for the numerical one, a fourth-order centered scheme with a step $\Delta\sigma = 10^{-3}$ is used.

where the k-th coefficient is given by:

$$\boldsymbol{d}_k(t) = \frac{1}{l}\int_0^l \mathrm{d}s\ \boldsymbol{\tau}(s,t)\ \partial_{\boldsymbol{x}}\overline{\boldsymbol{u}}[\boldsymbol{x}(s,t)]\ \mathrm{e}^{-\mathrm{i}\,\mathrm{K}\,s} \tag{31}$$

and, the patch boundary ∂P being a closed curve, $\boldsymbol{d}_0 \equiv 0$. From the representation (30), the relative elongation velocity $\Lambda = \dot{l}/l$, which is also the mean value of the periodic function $\partial_s\dot{s}$, may be easily evaluated as follows:

$$\Lambda = \frac{1}{l}\int_0^l \mathrm{d}s\ \partial_s\dot{s} = \frac{\mathrm{i}}{2}\sum_p \mathrm{P}\ (\boldsymbol{c}_p\,\boldsymbol{d}_{-p} - \overline{\boldsymbol{c}}_p\,\overline{\boldsymbol{d}}_{-p}), \tag{32}$$

in which Equations (11) and (4) are also used. From Equations (4, 32) and the definition of the function v (10), it is also deduced that the k-th Fourier coefficient, for $k \neq 0$, of v is the following:

$$\boldsymbol{v}_k = \frac{\mathrm{i}}{2} \sum_p {}^{\mathrm{P}} \left(\boldsymbol{c}_p \, \boldsymbol{d}_{k-p} - \overline{\boldsymbol{c}}_p \, \overline{\boldsymbol{d}}_{-k-p}\right), \tag{33}$$

while $\boldsymbol{v}_0 = 0$. Note also that $\overline{\boldsymbol{v}}_k = \boldsymbol{v}_{-k}$.[4]

By accounting for the relations (12, 13) and inserting the identity (14) into $\boldsymbol{X}_k$, Equation (9) leads to the following differential problem for the Fourier coefficients:

$$\begin{cases} \dot{\boldsymbol{c}}_0 \;=\; \boldsymbol{\mu} + \dfrac{\mathrm{i}}{2} \displaystyle\sum_{\substack{p,\,q \\ p \neq 0}} {}^{\mathrm{Q}} \, \boldsymbol{c}_p \, \left(\boldsymbol{c}_q \, \boldsymbol{d}_{-p-q} - \overline{\boldsymbol{c}}_q \, \overline{\boldsymbol{d}}_{p-q}\right) \\ \dot{\boldsymbol{c}}_k \;=\; \dfrac{\mathrm{i}}{2} \Bigg[\; {}^{\mathrm{K}} \, \boldsymbol{c}_k \displaystyle\sum_{\substack{p,\,q \\ p \neq q}} \frac{{}^{\mathrm{P}}}{{}^{\mathrm{P}} - {}^{\mathrm{Q}}} \left(\boldsymbol{c}_p \, \boldsymbol{d}_{-q} + \overline{\boldsymbol{c}}_p \, \overline{\boldsymbol{d}}_{-q}\right) + \\ \qquad\qquad + \displaystyle\sum_{\substack{p,\,q \\ p \neq k}} \frac{{}^{\mathrm{P}} \, {}^{\mathrm{Q}}}{{}^{\mathrm{P}} - {}^{\mathrm{K}}} \, \boldsymbol{c}_p \, \left(\boldsymbol{c}_q \, \boldsymbol{d}_{k-p-q} - \overline{\boldsymbol{c}}_q \, \overline{\boldsymbol{d}}_{-k+p-q}\right) \Bigg] - \mathrm{i} \, \dfrac{\overline{\boldsymbol{d}}_{-k}}{{}^{\mathrm{K}}}, \end{cases} \tag{34}$$

where the case of $k = 0$ must be distinguished from the others. Note also that the right-hand sides of all Equations (34) do not contain the coefficient $\boldsymbol{c}_0$, so that $\boldsymbol{c}_0$ depends on all the other coefficients $\boldsymbol{c}_k$, but these latter ones do not depend on $\boldsymbol{c}_0$. Finally, in the first equation of the system (34) $\boldsymbol{\mu}$ is the following function of time:

$$\boldsymbol{\mu} = \dot{\boldsymbol{x}}_0 - \mathrm{i} \sum_{k \neq 0} \frac{\overline{\boldsymbol{d}}_k}{{}^{\mathrm{K}}}. \tag{35}$$

As stated above, the time integration of the system (34) needs the Fourier coefficients (31) of the tangent derivative of the velocity, given the corresponding coefficients for the patch shape. For example, in the case of an elliptical patch, with axis ratio $\lambda = a/b$ and angular velocity of the contour ∂P given by $\Omega = \lambda/(\lambda + 1)^2$, the relation between those Fourier coefficients may be written in the simple form:

$$\boldsymbol{d}_k = \frac{{}^{\mathrm{K}}}{2} \left[\overline{\boldsymbol{c}}_{-k} - \frac{\lambda - 1}{\lambda + 1} \, \mathrm{e}^{-2 \, \mathrm{i} \, \theta(t)} \, \boldsymbol{c}_k \right].$$

where $\theta(t) = \theta_0 + \Omega \, t$ is the phase of the semi-axis a, at the numerator of λ. In the general case, the link between the patch shape and the tangent derivative of the velocity is not so simple. However, for a nearly circular patch, from the definition (31) of the k-th Fourier coefficient $\boldsymbol{d}_k$ and the series representation (23) of the tangent derivative of the velocity, the following form of the coefficient $\boldsymbol{d}_k$ is obtained:

$$\boldsymbol{d}_k = -\frac{{}^{\mathrm{K}}}{2} \sum_{m=1}^{\infty} \frac{1}{m} \, \boldsymbol{a}_{m+1} \, \boldsymbol{e}_{k,m}, \tag{36}$$

[4] With regard to the primitive function w, it is worth noticing that the sum of its Fourier coefficients vanishes, from the conditions $w(0) = w(l) = 0$. Its Fourier coefficients are given by:

$$\boldsymbol{w}_k = -\mathrm{i} \, \frac{\boldsymbol{v}_k}{{}^{\mathrm{K}}} \quad \text{for } k \neq 0, \text{ while:} \quad \boldsymbol{w}_0 = \mathrm{i} \sum_{k \neq 0} \frac{\boldsymbol{v}_k}{{}^{\mathrm{K}}}.$$

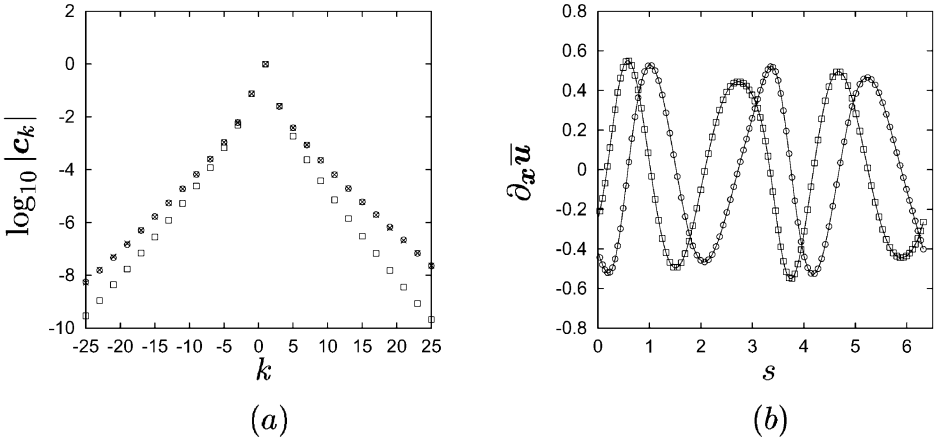

Figure 7. For a patch of kind (28) with $n = 2$ and $\varepsilon = 0{\cdot}2$, in (a) the logarithm of the modulus of the Fourier coefficients $\boldsymbol{c}_k$ is drawn *vs.* k at the initial time (squares) and at time 3, from the contour dynamics simulation (crosses) and the present spectral approach (circles). The integration is carried out with a fourth-order Runge-Kutta scheme with time step 0·01. Relative errors on the area A and on the second-order moment I are smaller than 3×10^{-8} and 6×10^{-8}, respectively. In (b) the tangential (squares) and normal (circles) components of the tangent derivative $\partial_{\boldsymbol{x}}\overline{\boldsymbol{u}}$ are drawn *vs.* the arc length s; they are evaluated numerically (solid line), via the contour dynamics velocity (1), and by the series (23), with 140 terms.

where $\boldsymbol{a}_m$, for $m \geq 2$, is the m-th coefficient (24) of the Laurent series of the function $\boldsymbol{\phi}$ and the definition (15) of $\boldsymbol{e}_{k,m}$ has been used. The Laurent coefficients in Equation (36) are evaluated by introducing the modified (for a translation of $\boldsymbol{\alpha}$) Fourier coefficient of the patch shape $\tilde{\boldsymbol{c}}_p$, which is equal to $\boldsymbol{c}_p$ for all $p \neq 0$, while $\tilde{\boldsymbol{c}}_0 = \boldsymbol{c}_0 - \boldsymbol{\alpha}$. Moreover, it is also needed to consider the Fourier coefficients $\tilde{\boldsymbol{c}}_k^{(m+1)}$ for the $(m+1)$-th power of $\boldsymbol{x} - \boldsymbol{\alpha}$, evaluated as:

$$\tilde{\boldsymbol{c}}_k^{(m+1)} = \sum_p \tilde{\boldsymbol{c}}_p \, \tilde{\boldsymbol{c}}_{k-p}^{(m)},$$

starting from the ones for $m = 1$. In terms of these coefficients, $\boldsymbol{a}_m$ is given as:

$$\boldsymbol{a}_m = -\sum_p p \, \overline{\boldsymbol{c}}_p \, \tilde{\boldsymbol{c}}_p^{(m-1)}.$$

The coefficients $\boldsymbol{e}_{k,m}$ in Equation (36) are evaluated by integrating in time the evolution equation for $\boldsymbol{e}_{k,1}$:

$$\dot{\boldsymbol{e}}_{k,1} = \sum_p (v_p - \mathrm{i}\,\mathrm{K}\, w_p)\, \boldsymbol{e}_{k-p,1} + \mathrm{i} \sum_{\substack{p,\,q \\ q \neq 0}} \frac{\mathrm{P}(\mathrm{K}+\mathrm{P}+\mathrm{Q})}{\mathrm{Q}} \, \overline{\boldsymbol{c}}_p \, \overline{\boldsymbol{d}}_q \, \boldsymbol{e}_{k+p+q,1} + \tag{37}$$

$$+\boldsymbol{\mu} \sum_p \mathrm{P}\,(\mathrm{K}+\mathrm{P})\, \overline{\boldsymbol{c}}_p \, \boldsymbol{e}_{k+p,1},$$

which follows from Equation (16), by using the Fourier series (30) for the tangent derivative of the velocity and the definition (35) of $\boldsymbol{\mu}$. Then, each remaining coefficient $\boldsymbol{e}_{k,m+1}$, for $m \geq 1$, is obtained through the recurrence formula:

$$\boldsymbol{e}_{k,m+1} = -\frac{1}{m} \sum_p \mathrm{P}\,(\mathrm{K}+\mathrm{P})\, \overline{\boldsymbol{c}}_p \, \boldsymbol{e}_{k+p,m},$$

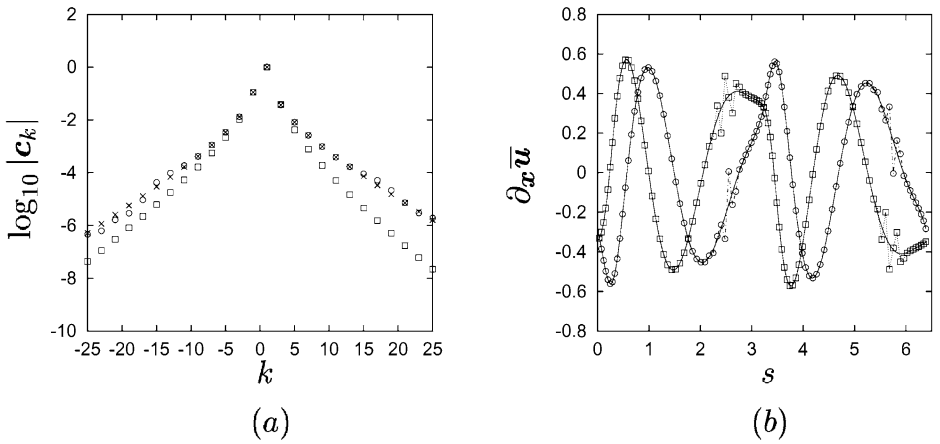

Figure 8. As in Figure 7, with $\varepsilon = 0{\cdot}3$. Relative errors on the area A and on the second order moment I are smaller than 2×10^{-7} and 4×10^{-7}, respectively. Note the lack of convergence of the series of $\partial_{\boldsymbol{x}} \overline{\boldsymbol{u}}$ (b), which induces the errors on the Fourier coefficients at time 3, shown in (a).

starting from the ones $\boldsymbol{e}_{k,1}$.

The spectral formulation is validated by a comparison with the numerical simulation of the vortex motion carried out with the contour dynamics algorithm. Moreover, the same two first integrals of the motion (the area and the second-order moment of the patch) are evaluated during the time integration of the system (34, 37). The differences between their initial values and the current ones are assumed as global measures of the accuracy of the numerical integration. The area A of the patch is written in terms of the Fourier coefficients of its shape as:

$$A = \pi \sum_p p \, \boldsymbol{c}_p \overline{\boldsymbol{c}}_p,$$

while the second-order moment is written:

$$I = \frac{\pi}{2} \, \mathfrak{Re}\left[\sum_{q,r,p} (q + r - p) \, \boldsymbol{c}_q \boldsymbol{c}_r \overline{\boldsymbol{c}}_p \overline{\boldsymbol{c}}_{q+r-p} \right].$$

As a sample of vortex dynamics which may be treated with the present approach, for a patch of the kind (28) with $n = 2$ and ε sufficiently small, in Figure 7a the logarithm of the modulus of the Fourier coefficients $\boldsymbol{c}_k$ is drawn *vs.* k at the initial time and at time 3, from the contour dynamics simulation and the present spectral method, with 51 Fourier coefficients. A satisfactory agreement is obtained, even if the truncation of the series leads to growing errors at later times. To verify the convergence of the series for the tangent derivative of the velocity at the final time 3, in Figure 7b the tangential and normal components of $\partial_{\boldsymbol{x}} \overline{\boldsymbol{u}}$ are drawn *vs.* the arc length s, through a fourth-order numerical derivative of the contour dynamics velocity (1) and by the series (23). It happens that the boundary deformations at that time are quite small, so that the Laurent series for $\boldsymbol{\phi}$ results still convergent. On the contrary, by repeating the simulation for a larger ε, the convergence of that series at time 3 is lost (see Figure 8b) and the present spectral approach does not work at later times.

8. Concluding remarks and perspectives

The present paper deals with the motion of a two-dimensional, uniform vortex in an inviscid, isochoric fluid, by looking at the time behaviour of intrinsic quantities related to its boundary, such as tangent unit vector, curvature and Fourier coefficients for the vortex shape. In this analysis, a relevant role is played by the tangent derivative of the velocity along the boundary. It depends on the analytic continuation of the function $\boldsymbol{\phi} = 1/\boldsymbol{\tau}^2$ outside the boundary itself, through a standard Cauchy integral. The present approach may be also viewed as extending a classical one, based on the Schwarz function $\boldsymbol{\Phi}$ of the vortex boundary, to any (smooth) vortex shape.

A few sample cases have been investigated analytically, in order to show the feasibility of the present formulation. In this regard, the study of the evolution in time of the singularities (as branch cuts or poles) of $\boldsymbol{\phi}$ will be the object of future work, by starting from the present highly non-trivial analytical solutions.

For a class of nearly circular vortices, the function $\boldsymbol{\phi}$ of which may be expanded in a Laurent series on the boundary, it is also found that the tangent derivative of the velocity is given by the singular part of such a series. An extremely simple and suggestive relation between vortex shape and self-induced boundary velocities is obtained. Moreover, for such vortices, the time evolution of the Fourier coefficients for the vortex shape may also be investigated by a spectral approach, which holds until the boundary deformations remain sufficiently small. In the author's opinion, the present spectral approach does not replace that involving contour dynamics. Nevertheless, it promises to be useful in order to study the interactions between different wave numbers, due to the strongly nonlinear nature of the problem. This point is one of the main issues of future investigations.

Unfortunately, in the general case, the relation between Fourier coefficients and tangent derivative of the velocity cannot be handled so simply. A deeper analysis still seems to be necessary. For example, by using the Fourier representation (8), the tangent derivative of the velocity (18) may be evaluated in the plane of the new complex variable $z = \exp(\mathrm{i}\, 2\pi\ s/l)$ (note that ∂P maps onto the unit circle $\partial \mathcal{C}$ in the z-plane). As a matter of fact, if the vortex boundary is approximated by:

$$\boldsymbol{x}(z) \simeq \sum_{k=-m_1}^{+m_2} \boldsymbol{c}_k\ z^k,$$

for $z \in \partial \mathcal{C}$ and suitable positive integers $m_{1,2}$, the limit (19) may be evaluated as:

$$\boldsymbol{V}(z) \simeq \frac{1}{2\pi\,\mathrm{i}} \lim_{r \to 0^+} \int_{\partial C_r(z)} \mathrm{d}\boldsymbol{\zeta}\ \boldsymbol{\zeta}^{m_1-m_2-1}\ \frac{p_{m_1m_2}(\boldsymbol{\zeta})}{q_{m_1m_2}(\boldsymbol{\zeta}; z)},$$

where the two following polynomials in $\boldsymbol{\zeta}$:

$$\begin{aligned} \boldsymbol{p}_{m_1m_2}(\boldsymbol{\zeta}) &= \sum_{k=0}^{m_1+m_2} (m_2 - k)\ \overline{\boldsymbol{c}}_{m_2-k}\ \boldsymbol{\zeta}^k \\ \boldsymbol{q}_{m_1m_2}(\boldsymbol{\zeta}; z) &= \sum_{l=0}^{m_1+m_2} \boldsymbol{c}_{l-m_1}\ \boldsymbol{\zeta}^l - \boldsymbol{x}(z)\ \boldsymbol{\zeta}^{m_1} \end{aligned}$$

have been introduced. In this way, the tangent derivative of the velocity in the point $\boldsymbol{x}(z)$ follows from the (numerical) solution in ζ of the $(m_1 + m_2)$-th degree algebraic equation:

$$\boldsymbol{q}_{m_1 m_2}(\zeta; z) = 0,$$

by the residue theorem. This approach appears still unsatisfactory, because the roots of the above equation depend on z and, as a consequence, different equations must be solved for different z on $\partial\mathcal{C}$.

9. Appendix Technical details about the analytical evaluation of the tangent derivative in sample cases

In the present appendix, details about the analytical evaluation of the function (19) for the sample cases considered in Section 6 are summarized.

9.1. The elliptical patch

In the physical plane, the tangent derivative of the boundary velocity may be calculated by applying the external residue theorem to the integral (19), with the definition (27) of the function $\boldsymbol{\phi}$. Accounting for the residual values $\mathrm{Res}(\boldsymbol{x}) = -\boldsymbol{\phi}(\boldsymbol{x})$ and $\mathrm{Res}(\infty) = (\lambda - 1)/(\lambda + 1)$, one has:

$$\boldsymbol{V}(\boldsymbol{x}) = -\left[\mathrm{Res}(\boldsymbol{x}) + \mathrm{Res}(\infty)\right] = -\frac{4\lambda}{\lambda + 1}\,\frac{1}{(\lambda + 1)z^2 - (\lambda - 1)}. \tag{A1}$$

On the contrary, by using the Cauchy theorem inside the vortex, the following definition of $\boldsymbol{V}$ is obtained:

$$\boldsymbol{V}(\boldsymbol{x}) = -\frac{2\lambda}{\pi(\lambda^2 - 1)}\int_{-c}^{+c} \mathrm{d}\xi\,\frac{\xi}{\sqrt{c^2 - \xi^2}}\,\frac{1}{\boldsymbol{x} - \xi},$$

which is evaluated through the identity:

$$\int_{-c}^{+c} \mathrm{d}\xi\,\frac{\xi}{\sqrt{c^2 - \xi^2}}\,\frac{1}{\boldsymbol{x} - \xi} \equiv -\underbrace{\int_{-c}^{+c}\frac{\mathrm{d}\xi}{\sqrt{c^2 - \xi^2}}}_{I_1} + |\boldsymbol{x}|^2\underbrace{\int_{-c}^{+c}\frac{\mathrm{d}\xi}{\sqrt{c^2 - \xi^2}}\,\frac{1}{(x - \xi)^2 + y^2}}_{I_2} + \\ -\boldsymbol{x}\underbrace{\int_{-c}^{+c}\frac{\mathrm{d}\xi}{\sqrt{c^2 - \xi^2}}\,\frac{\xi}{(x - \xi)^2 + y^2}}_{I_3},$$

where the integrals in the right-hand side of the above equation are:

$$I_1 = \pi, \quad I_2 = \frac{\pi\lambda}{\dfrac{x^2}{\lambda^2} + \lambda^2 y^2}, \quad I_3 = \pi\,\frac{\lambda^2 - 1}{\lambda}\,\frac{x}{\dfrac{x^2}{\lambda^2} + \lambda^2 y^2},$$

still leading to the result (A1).

In the transformed z-plane, the limit $\boldsymbol{V}$ (19) is evaluated in the following terms:

$$\boldsymbol{V}(z) = -\frac{1}{2\pi\,\mathrm{i}}\lim_{r\to 0^+}\int_{\partial C_r(z)} \mathrm{d}\zeta\,\frac{\gamma^2\zeta^2 - 1}{\zeta\,(\zeta - z)\,(\zeta - \gamma^2/z)},$$

with the internal residue theorem ($\mathrm{Res}(0) = -1/\gamma^2$, $\mathrm{Res}(\gamma^2/z) = (\gamma^6 - z^2)/[\gamma^2\,(\gamma^2 - z^2)]$) or with the external one ($\mathrm{Res}(\infty) = -\gamma^2$, $\mathrm{Res}(z) = (\gamma^2 z^2 - 1)/(z^2 - \gamma^2)$), leading always to the result (A1).

9.2. The multipolar patches (28)

In the present section, the analytical evaluation of the limit (19) is carried out for a patch having its boundary defined through Equation (28), for an arbitrary n. Some definitions simplify the analysis below. The angle which parameterizes ∂P is called θ in the independent variables ($\boldsymbol{x}$: physical plane, z: transformed one) and τ in the dependent ones ($\boldsymbol{y}$, $\boldsymbol{\zeta}$). The patch shape (28) is a periodic function of θ, with a period $2\pi/n$, so it is convenient to introduce the angle $\alpha = \pi/n$. The n-th roots of the unit $\boldsymbol{\chi}_k = \exp(\mathrm{i}\,\Theta_k)$ with $\Theta_k = 2\,k\,\alpha$ for $k = 0, 1, \ldots, n-1$ are employed, also with the useful extensions $\Theta_n = 2\,n\,\alpha = 2\pi$ and $\boldsymbol{\chi}_n = \boldsymbol{\chi}_0$.

First of all, in Equation (28) the map $\boldsymbol{x} = \boldsymbol{x}(z)$ is inverted:

$$z^n = \frac{1}{\varepsilon}\,(1 \pm 2\delta^{n/2}\sqrt{\mu^n - \boldsymbol{x}^n}), \tag{A2}$$

where the branch of the square root having argument in $[0, \pi)$, has been used. As a consequence, the choice of the sign in Equation (A2) depends on the phase of $\boldsymbol{x}^n$: the sign "+" holds for $\arg(\boldsymbol{x}) \in (\Theta_k, \Theta_k + \alpha)$, while the sign "−" for $\arg(\boldsymbol{x}) \in \left[\Theta_k + \alpha, \Theta_{k+1}\right]$, where the integer k runs from 0 to $n-1$. Finally, among the n-th roots of z^n, which follow from Equation (A2), only the one for which $\arg(z) = \arg(\boldsymbol{x})$ must be considered, as implied by Equation (28).

As a second step, the function $\boldsymbol{\phi}$ is evaluated in the z-plane, leading to the following definition of the limit $\boldsymbol{V}$ (19):

$$\boldsymbol{V}(z) = \frac{1}{\varepsilon\,\pi\,\mathrm{i}} \lim_{r \to 0^+} \int_{\partial \mathcal{C}_r(z)} \frac{\mathrm{d}\boldsymbol{\zeta}}{\boldsymbol{\zeta}^3}\, \frac{\varepsilon - \boldsymbol{\zeta}^n}{(\boldsymbol{\zeta}^n - z^n)\,(\boldsymbol{\zeta}^n - \boldsymbol{\Xi}^n)} \sum_{h=0}^{n-1} \left[\, \frac{\boldsymbol{x}(z)}{\boldsymbol{y}(\boldsymbol{\zeta})} \,\right]^h, \tag{A3}$$

in which $\boldsymbol{\Xi}^n = 1/\delta^n - z^n$ and $\boldsymbol{y}^n(\boldsymbol{\Xi}) = \boldsymbol{x}^n(z)$. The singular points of the function under the integral in the right-hand side of Equation (A3) are the following: *I*) the pole of order 3 in the origin ($\boldsymbol{\zeta} = 0$); *II*) for $n \geq 2$, the branch points of the function $\boldsymbol{y}(\boldsymbol{\zeta})$; *III*) the n-th roots of z^n, given by $\boldsymbol{\chi}_k z$ for $k = 0, 1, \ldots, n-1$; and, finally, *IV*) the n-th roots of $\boldsymbol{\Xi}^n$, which are outside $\partial\mathcal{C}$. The branch points of the function $\boldsymbol{y}(\boldsymbol{\zeta})$ are located in $\boldsymbol{\chi}_k p$, $\boldsymbol{\chi}_k q$ for $k = 0, 1, \ldots, n-1$, having defined the two positive constants p and q as the real and positive n-th roots of the quantities:

$$p^n = \frac{1 - \sqrt{1 - \varepsilon^2}}{\varepsilon} < 1, \quad q^n = \frac{1 + \sqrt{1 - \varepsilon^2}}{\varepsilon} > 1, \tag{A4}$$

with $p\,q = 1$. However, the singularities of kind *III* for $k \geq 1$ are only apparent, because $\boldsymbol{y}(\boldsymbol{\chi}_k z) = \boldsymbol{\chi}_k \boldsymbol{x}(z)$ and, as a consequence, the sum $1 + \boldsymbol{x}/\boldsymbol{y} + (\boldsymbol{x}/\boldsymbol{y})^2 + \ldots + (\boldsymbol{x}/\boldsymbol{y})^{n-1}$ vanishes. On the contrary, this latter sum holds n, for $k = 0$.

The function $\boldsymbol{y}$, which gives the vortex shape in the transformed $\boldsymbol{\zeta}$-plane, may be written as the following product:

$$\boldsymbol{y}(\boldsymbol{\zeta}) = \delta\, e^{\mathrm{i}\,m\,\pi/n} \prod_{k=0}^{n-1} [\boldsymbol{\chi}_{n-k}\,(\boldsymbol{\zeta} - \boldsymbol{\chi}_k p)]^{1/n}\, [\boldsymbol{\chi}_{n-k}\,(\boldsymbol{\chi}_k q - \boldsymbol{\zeta})]^{1/n}, \tag{A5}$$

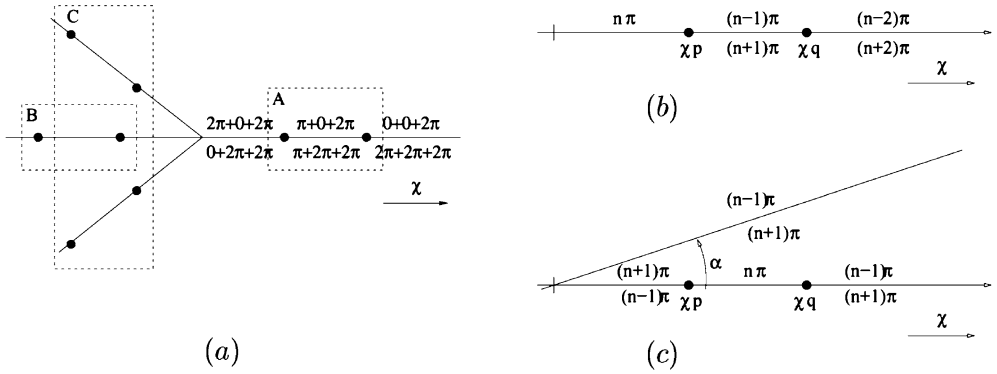

Figure 9. In (*a*) the phase contributions (A7) along a direction $\boldsymbol{\chi} = \exp(\mathrm{i}\,\Theta)$ (one among $\boldsymbol{\chi}_0, \boldsymbol{\chi}_1, \ldots, \boldsymbol{\chi}_{n-1}$) due to the branch points $\boldsymbol{\chi} p$ and $\boldsymbol{\chi} q$ (*A*, first numbers in the sums), to the ones along $-\boldsymbol{\chi}$ (*B*, second numbers, present only for *n* even) and to the branch points along a couple of symmetrical directions (*C*, third numbers) are evaluated. In particular, for *n* even, $(n-2)/2$ of the latter contributions are present in the sum (A7), while, for *n* odd, they are $(n-1)/2$. In (*b*) and (*c*) there are the whole phases along $\boldsymbol{\chi}$ for *n* even and odd, respectively. In the latter case, a jump along the direction $\Theta + \alpha$ is also present in the sum (A7).

where the relative integer m is even for n odd and odd for n even. Its argument, which must be equal to $\arg(\boldsymbol{\zeta})$ when $\boldsymbol{\zeta} \in \partial\mathcal{C}$, is evaluated by introducing the phases of the vectors joining $\boldsymbol{\chi}_k p$ and $\boldsymbol{\chi}_k q$ with $\boldsymbol{\zeta}$:

$$\begin{aligned} \alpha_k &= \arg[\boldsymbol{\chi}_{n-k}(\boldsymbol{\zeta} - \boldsymbol{\chi}_k p)] \in [0, 2\pi) \\ \beta_k &= \arg[\boldsymbol{\chi}_{n-k}(\boldsymbol{\zeta} - \boldsymbol{\chi}_k q)] \in [-\pi, +\pi) \end{aligned} \tag{A6}$$

relative to the $\boldsymbol{\chi}_k$ direction, for $k = 0, 1, \ldots, n-1$. Here, α_k and β_k belong to different ranges: the first one runs from 0 (included) to 2π, *i.e.*, it is the principal argument of $\boldsymbol{\chi}_{n-k}(\boldsymbol{\zeta} - \boldsymbol{\chi}_k p)$, while, to obtain the same range of variation for the phase of $\boldsymbol{\chi}_{n-k}(\boldsymbol{\chi}_k q - \boldsymbol{\zeta})$ in Equation (A5), the phase β_k must run from $-\pi$ (included) to $+\pi$. The two cuts, induced by the different phase definitions, have opposite directions, so it becomes possible, via a particular choice of the branches of the factors in Equation (A5), to obtain a phase for the whole function $\boldsymbol{y}(\boldsymbol{\zeta})$ which results continuous across the segment joining $\boldsymbol{\chi}_k p$ with $\boldsymbol{\chi}_k q$. Being $p < 1$ and $q > 1$, such a phase will be also continuous on the unit circle $\partial\mathcal{C}$.

The phase of the function $\boldsymbol{y}$ may be written in terms of the arguments given in Equation (A6) and the following sum:

$$\sum_{r=0}^{n-1} (\alpha_r + \beta_r) \tag{A7}$$

along each direction $\boldsymbol{\chi}_k$ (for $\boldsymbol{\zeta} = s\exp(\mathrm{i}\,\tau)$, with $\tau = \Theta_k = 2k\alpha$ and $s > 0$) is considered, starting from the case in which n is even. From Figure 9a it is found that the phase (A7) is $n\pi$ for $0 < s < p$, $(n+1)\pi$ for $p < s < q$ and $\tau = \arg\boldsymbol{\zeta} = \Theta_k^-$, $(n-1)\pi$ for $\tau = \Theta_k^+$, $(n+2)\pi$ for $s > q$ and $\tau = \Theta_k^-$, $(n-2)\pi$ for $\tau = \Theta_k^+$; see also Figure 9b. As a consequence, by assuming $m = -(n-1)$ in Equation (A5), $\arg\boldsymbol{y}(\boldsymbol{\zeta})$ is written for n even as:

$$\arg\boldsymbol{y}(\boldsymbol{\zeta}) = -(n-1)\,\alpha + \frac{1}{n}\sum_{r=0}^{n-1} (\alpha_r + \beta_r) + 2\,h\,\alpha,$$

where the integer h turns out to be equal to k, if $\tau \in [\Theta_k, \Theta_{k+1})$, for $k = 0, \ldots, n-1$. In this way, arg $\boldsymbol{y}(\boldsymbol{\zeta})$ along the direction $\boldsymbol{\chi}_k$ (*i.e.*, $\tau = \Theta_k$) is Θ_k for $p < s < q$, while it is given by $\Theta_k + \alpha$ for $0 < s < p$, $\tau = \Theta_k^+$ and for $s > q$, $\tau = \Theta_k^-$, while it is $\Theta_k - \alpha$ for $0 < s < p$, $\tau = \Theta_k^-$ and for $s > q$, $\tau = \Theta_k^+$.

For n odd, by using Figure 9a (without the contributions in B), the sum (A7) along each direction $\boldsymbol{\chi}_k$ (for $\boldsymbol{\zeta} = s\ \exp(\mathrm{i}\,\tau)$, $s > 0$ and $\tau = \Theta_k$) is $(n+1)\pi$ for $0 < s < p$ and $\tau = \Theta_k^+$, $(n-1)\pi$ for $\tau = \Theta_k^-$, $n\pi$ for $p < s < q$, $(n-1)\pi$ for $s > q$ and $\tau = \Theta_k^+$, $(n+1)\pi$ for $\tau = \Theta_k^-$; see also Figure 9c. As shown in that figure, for n odd, another phase discontinuity takes place across each direction exp[i $(\Theta_k + \alpha)$], for $k = 0, 1, \ldots, n-1$. Actually, the above direction is aligned, for $0 \le k \le (n-1)/2$, with $\boldsymbol{\chi}_{k+(n+1)/2}$ and, for $(n+1)/2 \le k \le n-1$, with $\boldsymbol{\chi}_{k-(n-1)/2}$. The resulting sum (A7) on the line $\tau = \Theta_k + \alpha$ may be evaluated starting from Figure 9a, without considering the contributions in A (first numbers in the sums in the figure). A jump from $(n+1)\pi$ for $\tau = (\Theta_k + \alpha)^-$ to $(n-1)\pi$ for $\tau = (\Theta_k + \alpha)^+$ is found, see also Figure 9c. It follows that arg $\boldsymbol{y}(\boldsymbol{\zeta})$, by choosing $m = -2n$ in Equation (A5), may be written as:

$$\arg \boldsymbol{y}(\boldsymbol{\zeta}) = -\pi + \frac{1}{n} \sum_{r=0}^{n-1} (\alpha_r + \beta_r) + 2\, h\, \alpha,$$

where the integer h is fixed at 0 when $\tau \in [0, \alpha)$, k when $\tau \in [\Theta_k - \alpha, \Theta_k + \alpha)$ for $k = 1, 2, \ldots, n-1$ and n when $\tau \in [\Theta_n - \alpha, 2\pi)$. In this way, arg $\boldsymbol{y}(\boldsymbol{\zeta})$ in the directions $\boldsymbol{\chi}_k$ behaves as in the case of n even and the jumps along the directions $\Theta_k + \alpha$ disappear.

In the selected branch of the function $\boldsymbol{y}$, the discontinuities outside the unit circle $\partial\mathcal{C}$ are only along the directions $\boldsymbol{\chi}_k$, for $|\boldsymbol{\zeta}| > q$. When the internal residue theorem is applied to evaluate the limit (A3), the integration along these directions leads to the following quantity:

$$\begin{aligned} &\frac{1}{\varepsilon\ \pi\ \mathrm{i}} \sum_{m=0}^{n-1} \boldsymbol{x}^m \int_q^{+\infty} \frac{\mathrm{d}\xi}{\xi^3}\ \frac{\varepsilon - \xi^n}{(\xi^n - \boldsymbol{z}^n)\ (\xi^n - \boldsymbol{\Xi}^n)}\ \frac{1}{|\boldsymbol{y}(\xi)|^m} \times \\ &\qquad \times \sum_{k=0}^{n-1} \mathrm{e}^{-2\,\mathrm{i}\,\Theta_k} \left[\mathrm{e}^{-\mathrm{i}\,(\Theta_k + \alpha)\,m} - \mathrm{e}^{-\mathrm{i}\,(\Theta_k - \alpha)\,m} \right], \end{aligned} \tag{A8}$$

where the last sum, which depends on the phase jumps of the function $\boldsymbol{y}(\boldsymbol{\zeta})$, does not vanish if and only if $m = n - 2$, when it holds $-2\,\mathrm{i}\,n\ \sin[(n-2)\pi/n]$.

To evaluate the integral in the sum (A8) for $m = n - 2$, the following quantity has to be considered:

$$\mathcal{I}(\gamma, \sigma; s, v, w) = \int_0^1 \mathrm{d}\xi\ \frac{\xi^\gamma\ (s - \xi)^{-\sigma}\ (1 - \xi)^{-\sigma}}{\xi^2 - 2vw\xi + w^2}, \tag{A9}$$

γ, σ, s, v and w being suitable real numbers. The case $\gamma > 0$, $0 < \sigma < 1$, $|v| < 1$ for any w and $|v| = 1$ only for $|w| > 1$ is considered below, in such a way that the second-degree polynomial in the denominator in Equation (A9) is positive for any $\xi \in [0, 1]$. Moreover, the integral (A9) is evaluated numerically with a second-order scheme, after a preliminary integration by parts, to avoid the singularity in $\xi = 1$ of the factor $(1 - \xi)^{-\sigma}$. In terms of the following quantities:

$$
\begin{aligned}
j_1^{(n)}(\theta) &= \mathfrak{Re}(z^n) = \cos n\theta, \\
j_2^{(n)}(\theta) &= \frac{\mathfrak{Re}(\Xi^n)}{|\Xi^n|} = \frac{2 - \varepsilon\cos n\theta}{(4 + \varepsilon^2 - 4\varepsilon\cos n\theta)^{1/2}}, \\
j_3^{(n)}(\theta) &= \frac{q^n}{|\Xi^n|} = \frac{1 + \sqrt{1 - \varepsilon^2}}{(4 + \varepsilon^2 - 4\varepsilon\cos n\theta)^{1/2}},
\end{aligned}
$$

the values of the integral (A9) which are needed are given by:

$$
\begin{aligned}
f_1^{(n)}(\theta) &= \mathcal{I}\left[\frac{2n-2}{n}, \frac{n-2}{n}; \frac{q^n}{p^n}, j_1^{(n)}(\theta), q^n\right], \\
f_2^{(n)}(\theta) &= \mathcal{I}\left[\frac{3n-2}{n}, \frac{n-2}{n}; \frac{q^n}{p^n}, j_1^{(n)}(\theta), q^n\right], \\
f_3^{(n)}(\theta) &= \mathcal{I}\left[\frac{2n-2}{n}, \frac{n-2}{n}; \frac{q^n}{p^n}, j_2^{(n)}(\theta), j_3^{(n)}(\theta)\right], \\
f_4^{(n)}(\theta) &= \mathcal{I}\left[\frac{3n-2}{n}, \frac{n-2}{n}; \frac{q^n}{p^n}, j_2^{(n)}(\theta), j_3^{(n)}(\theta)\right].
\end{aligned}
\tag{A10}
$$

Regarding the evaluation of the residuals outside the unit circle $\partial\mathcal{C}$, and fixing a root Ξ of $\Xi^n = 1/\delta^n - z^n$, the sum of the residuals in the points $\chi_k\,\Xi$ leads to the definition of the integers $l(k)$, belonging to the set $\{0, 1, \ldots, n-1\}$, such that $\boldsymbol{y}(\chi_k\,\Xi) = \chi_{l(k)}\,\boldsymbol{x}(z)$. As a consequence, the following useful result is obtained:

$$
\frac{1}{n}\sum_{k=0}^{n-1}\chi_k^{n-2}\sum_{m=1}^{n-1}\chi_{l(k)}^m = \frac{1}{\chi_{k^\star}^2},
$$

where $\boldsymbol{y}(\chi_{k^\star}\,\Xi) = \boldsymbol{x}(z)$. The sum of the residuals is evaluated through the above equation, so, by using also the functions (A10), the limit (A3) follows:

$$
\begin{aligned}
\boldsymbol{V}(z) = \frac{1}{\delta^n}\,\frac{1}{z^n - \Xi^n}\Bigg\{ & \frac{\varepsilon - \Xi^n}{\chi_{k^\star}^2\,\Xi^{n+2}} - \frac{\varepsilon - z^n}{z^{n+2}} + \\
& + \sin[(n-2)\,\alpha]\,\frac{\boldsymbol{x}^{n-2}(z)}{\pi\,\delta^{n-2}\,q^2}\left[\frac{\varepsilon - z^n}{z^n}\left(q^n\,z^n\,f_1^{(n)}(\theta) - f_2^{(n)}(\theta)\right) + \right. \\
& \left. + \frac{\Xi^n - \varepsilon}{\Xi^n}\left(\frac{\delta^n\,q^n\,z^n}{z^n - \delta^n}\,f_3^{(n)}(\theta) - f_4^{(n)}(\theta)\right)\right]\Bigg\},
\end{aligned}
\tag{A11}
$$

for an arbitrary n.

Acknowledgements

The author is greatly indebted to two anonymous Referees for many helpful suggestions. Moreover, the author would like to thank Sandro Iafrati and Carmine Golia for many fruitful discussions.

References

1. H. Lamb, *Hydrodynamics.* New York: Dover Publications (1932) 738 pp.
2. M.V. Melander, N.J. Zabusky and A.S. Styczek, A moment model for vortex interactions of the two-dimensional Euler equations. Part 1. Computational validation of a Hamiltonian elliptical representation. *J. Fluid Mech.* 167 (1986) 95–115.
3. B. Legras and D.G. Dritschel, The elliptical model of two-dimensional vortex dynamics. I: The basic state. *Phys. Fluids A* 3 (1990) 845–854.
4. M.V. Melander, N.J. Zabusky and J.C. McWilliams, Symmetric vortex merger in two dimensions: causes and conditions. *J. Fluid Mech.* 195 (1988) 303–340.
5. G. Riccardi and R. Piva, Motion of an elliptical vortex under rotating strain: conditions for asymmetric merging. *Fluid Dyn. Res.* 23 (1998) 63–88.
6. D.G. Dritschel, Contour dynamics and Contour Surgery: numerical algorithms for extended high-resolution modeling of vortex dynamics in two-dimensional, inviscid, incompressible flows. *Comp. Phys. Repts.* 10 (1989) 77–146.
7. N.J. Zabusky, M.H. Hughes and K.V. Roberts, Contour Dynamics for the Euler equations in two dimensions. *J. Comp. Phys.* 48 (1979) 96–106.
8. B. Legras and V. Zeitlin, Conformal dynamics for vortex motions. *Phys. Lett. A* 167 (1992) 265–271.
9. J. Jimenez, Linear stability of a non-symmetric, inviscid, Karman street of small uniform vortices. *J. Fluid Mech.* 189 (1988) 337–348.
10. P.G. Saffman, *Vortex Dynamics.* Cambridge: Cambridge University Press (1992) 311 pp.
11. D.G. Crowdy, A class of exact multipolar vortices. *Phys. Fluids* 11 (1999) 2556–2564.
12. D.G. Crowdy, Exact solutions for rotating vortex arrays with finite-area cores. *J. Fluid Mech.* 469 (2002) 209–235.
13. A.J. Majda and A.L. Bertozzi, *Vorticity and Incompressible Flow.* Cambridge: Cambridge University Press (2002) 632 pp.
14. D.I. Pullin, The nonlinear behaviour of a constant vorticity layer at a wall. *J. Fluid Mech.* 108 (1981) 401–421.